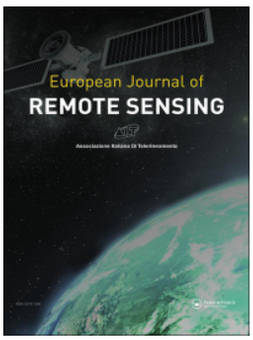

European Journal of Remote Sensing

ISSN: (Print) (Online) Journal homepage: https://www.tandfonline.com/loi/tejr20

Multi-spectral image change detection based on single-band iterative weighting and fuzzy C-means clustering

Liyuan Ma , Jia Zhenhong , Jie Yang & Nikola Kasabov

To cite this article: Liyuan Ma , Jia Zhenhong , Jie Yang & Nikola Kasabov (2020) Multi-spectral image change detection based on single-band iterative weighting and fuzzy C-means clustering, European Journal of Remote Sensing, 53:1, 1-13, DOI: 10.1080/22797254.2019.1707124

To link to this article: https://doi.org/10.1080/22797254.2019.1707124

EUROPEAN JOURNAL OF REMOTE SENSING
2020, VOL. 53, NO. 1, 1–13
https://doi.org/10.1080/22797254.2019.1707124

Multi-spectral image change detection based on single-band iterative weighting and fuzzy C-means clustering

Liyuan Ma[a], Jia Zhenhong[a], Jie Yang[b] and Nikola Kasabov[c]

[a]College of Information Science and Engineering, Xinjiang University, Urumuqi, China; [b]Institute of Image Processing and Pattern Recognition, Shanghai Jiao Tong University, Shanghai, China; [c]Knowledge Engineering and Discovery Research Institute, Auckland University of Technology, Auckland, New Zealand

ABSTRACT

In the present study, an improved iteratively reweighted multivariate alteration detection (IR-MAD) algorithm was proposed to improve the contribution of weakly correlated bands in multi-spectral image change detection. In the proposed algorithm, each image band was given a different weight through single-band iterative weighting, improving the correlation between each pair of bands. This method was used to obtain the characteristic difference in the diagrams of the band that contain more variation information. After removing Gaussian noise from each feature-difference graph, the difference graphs of each band were fused into a change-intensity graph using the Euclidean distance formula. Finally, unsupervised fuzzy C-means (FCM) clustering was used to perform binary clustering on the fused difference graphs to obtain the change detection results. By comparing the original multivariate alteration detection (MAD) algorithm, the IR-MAD algorithm and the proposed IR-MAD algorithm, which used a mask to eliminate strong changes, the experimental results revealed that the multi-spectral change detection results of the proposed algorithm are closer to the actual value and had higher detection accuracy than the other algorithms.

ARTICLE HISTORY
Received 13 July 2019
Revised 14 October 2019
Accepted 17 December 2019

KEYWORDS
Single-band iterative weighting; Multi-spectral change detection; IR-MAD; FCM clustering

Introduction

Remote sensing image change detection technology has been applied in many fields, such as environmental monitoring (Zhuang, Deng, & Fan, 2016), urban research (Zhuang, Deng, Yu, & Fan, 2017), land use (Yonezawa, 2007), sand cover monitoring (Yan-Hong, Pei, Wang, & Yun-Peng, 2010), forest monitoring (Zhuang, Deng, Fan, & Ma, 2018), agricultural investigation (Shi, Gao, & Shen, 2016), and disaster assessment (Chen & Chen, 2016). The change detection of remote sensing images is based on the multiple remote sensing images acquired at different time points in the same region to extract the features and process the changes in the ground objects. Because there are different structures and components between the objects, different features have different spectral characteristics, which means that the reflection spectra of different features are different. If the reflectance spectra of different objects are similar in some bands, the reflectance spectra of these objects in other bands will greatly differ. Single-band remote sensing image change detection can identify an object in a band but cannot extract the features of other wavelength change information. Furthermore, the multi-spectral remote sensing images of multiple wavelengths can reflect the characteristics of features under different wave bands and make good use of the spectral correlation. Moreover, the difference, as well as the change in the reaction features, can be more realistic (Hichri, Bazi, Alajlan, & Malek, 2013).

Due to the use of multi-spectral images for change detection, abundant spectral information can improve the credibility of identifying multiple types of changes. Hence, some targets that cannot be detected in a single band are more likely to be detected in multiple bands, which would be more conducive to understanding the change information of ground objects. The most critical part of change detection is change information discovery, and most studies have explored this issue (Zhang & Yang, 2005). To solve the deficiency of single-band change detection methods, such as the image ratio method (Xu, Zhang, He, & Guo, 2009), change vector analysis (CVA) (Liang, Wang, Sun, & Ying, 2017), and principal component analysis (PCA) (Hui, 2008), for multi-band remote sensing image change detection (suppressing noise, improving the detection accuracy, etc.), Nielsen et al. proposed the concept and method of MAD (Bai et al., 2012). The MAD algorithm is based on canonical correlation analysis (CCA) (Lei & Run-Geng, 2007). However, the algorithm could still not fully improve the deficiency of noise suppression and accuracy improvement in current multivariate remote sensing image processing schemes. Based on the MAD method, Nielsen also proposed the IR-MAD algorithm (Canty & Nielsen, 2008).

CONTACT Jia Zhenhong jzhh@xju.edu.cn Autonomous Region Key Laboratory of Signal and Information Processing, Xinjiang University, Urumuqi, China

A subsequent study (Nielsen & Canty, 2009) indicated that nuclear principal component analysis and nuclear MAF (the largest correlative factor) can further enhance the results after the implementation of the IR-MAD algorithm. In a prior study (Niemeyer, Marpu, & Nussbaum, 2008), the application of IR-MAD on image fragments, rather than on pixels, was demonstrated. In another study (Marpu, Gamba, & Canty, 2011), the IR-MAD method was proposed to eliminate strong changes to improve results. Strong changes refer to pixels that have clearly changed and are easily distinguishable. Strong changes can be obtained by the histogram difference method. By eliminating strong changes with a mask, the algorithm can better identify the background without changes. The mask here refers to the initial binary change mask calculated by identifying strong variations. By multiplying them by the image data matrix, the strongly varying pixels can be set to zero to eliminate the influence of strong changes on multi-spectral change detection in subsequent detection and reduce the amount of data processed. Although the iteration time and detection accuracy were improved, they could not make full use of the variation information of each band.

The IR-MAD algorithm has been considered the most advanced change detection algorithm for multi-spectral images due to its excellent change detection accuracy and varying stability. The main idea of IR-MAD is to assign an initial value of 1 to each pixel in the remote sensing images. During each iteration, a new weight is assigned to the two images by calculating the chi-square distribution probability. In the next iteration, weights are considered in the calculation of the mean and variance. Through these calculations, the pixels that do not change have large weights, and the weight of each pixel tends to be stable after iterative convergence. At this time, accurate change detection results can be obtained by comparing the weight and threshold of each pixel. Another theoretical explanation for IR-MAD was proposed in the literature (Wu & Du, 2015): multivariate change detection is the feature that seeks the strongest image correlation. This algorithm makes full use of the band with a strong correlation, while the band with a weaker correlation is given a smaller weight, which contributes less to the calculation of variation strength. Therefore, the IR-MAD algorithm fails to make full use of the variation characteristics of each band, resulting in the incomplete detection of the details of changed areas. Therefore, the algorithm has broken patches, much noise, and small change areas that are difficult to detect, and the overall detection rate is low (Xu, Liu, Li, Ren, & Yang, 2016). In recent years, with the development of machine learning methods, neural networks have also been applied to change detection in multi-spectral images. A common method is to take the difference image as the training labels and input them into a neural network, such as a convolutional neural network (CNN) (Jian, Fang, & Ghamisi, 2018; Maggiori, Tarabalka, Charpiat, & Alliez, 2016; Song, Li, Fang, & Lu, 2018), a generative adversarial network (GAN) (Gong, Niu, Zhang, & Li, 2017), a deep neural network (DNN) (Gong, Zhao, et al., 2017), a deep belief network (DBN) (Qiao, Pan, & Han, 2015), or a restricted Boltzmann machine (RBM) (Roux & Bengio, 2008). A novel recurrent convolutional neural network (ReCNN) architecture was later proposed to learn the combined spectral-temporal feature representation in a unified framework (Mou, Bruzzone, & Xiao, 2018). A generative discriminatory classified network (GDCN) consists of a discriminant classification network (DCN) and a generator (Gong, Yang, Zhan, Niu, & Li, 2019). These neural network models usually need to be trained by inputting a large amount of labelled data, which enables them to learn key feature representations from the input data. It is difficult and expensive to label a large amount data. Due to the lack of training data, network structure and high computational complexity, the application of neural networks in multi-spectral change detection is still being explored.

In the present study, a new, improved IR-MAD method for multi-spectral image change detection is proposed. In this algorithm, the image weights of each band were set to different weights to improve the correlation between each pair of bands of multi-spectral images. This method was used to obtain the characteristic difference diagrams of each band that contain more variation information. Because the noise in a multi-spectral image is mainly additive noise (such as Gaussian noise, Poisson noise, etc.), the Gaussian denoising algorithm is selected in this paper for the simple denoising of each feature-difference graph. (The comparison algorithm in this paper also includes the processing of Gauss filtering.) After Gaussian noise removal of each feature-difference graph, the difference graphs of each band were fused into a change-intensity graph using the Euclidean distance formula. Finally, unsupervised FCM binary clustering (Mishra, Ghosh, & Ghosh, 2012) was performed to obtain the change detection results. The results of experiments with the Landsat image dataset prove the superiority of the algorithm proposed in the present study. Moreover, compared with the detection results of the IR-MAD algorithm using MAD, IR-MAD and the latter-published IR-MAD algorithm using a mask to eliminate strong changes, the results reveal that the algorithm in the present study has a higher variation detection accuracy. Finally, the algorithm is discussed in terms of universality. The experiments of multiple sets of Landsat multi-spectral remote sensing datasets show that the proposed algorithm has good universality.

Methodology

The algorithm proposed in the present study comprises five steps:

Step 1: The original multi-spectral images are registered by ENVI software, and single-band images are separated.
Step 2: The single band is successively weighted by iterations to obtain the optimal projection vector of the upper two time phases of each band. The weight is calculated by Equation (7), and the optimal projection vector is calculated by Equations (1) and (2):
Step 3: Equation (5) is used to obtain the difference images of each band. Then, the obtained difference images are processed by Gaussian filtering;
Step 4: The difference image after filtering in each band is written into a matrix by Equation (8), and Equation (9) is used to convert the difference matrix into the MAD change-intensity matrix;
Step 5: Binary clustering analysis is performed with FCM clustering to obtain the change detection results.

The flow chart is shown in Figure 1.

The registration method

After acquiring multi-temporal remote sensing images for change detection, the most important pre-processing procedure is precise geometric registration. Because almost all remote sensing change detection research is based on the premise of image registration, a pixel in the image corresponds to the same geographical location in the real world. There are two main geometric registration methods for multi-temporal images: absolute registration of all images into real geographic coordinates and relative registration of corrected images. Absolute registration is more suitable for the change detection of large-scale multi-temporal data involving a large amount of data, but the accuracy of inter-image registration is affected by the cumulative accuracy of each individual correction. Relative registration is a method of relative correction by selecting the same points between images. This method is more suitable for the study of changes in terrain features with small amounts of data. This paper uses ENVI image registration and geometric correction tools to register pairs of images acquired in different time phases in the same area. The method is simple to operate, and the specific steps are as follows:

The flow chart is shown in Figure 2.

It should be noted that in the specific operation of generating matching points, the matching points should be found according to the default settings. In the specific operation of checking matching points, the generated matching points are sorted according to the error from largest to smallest. Matching Points with larger errors need to be deleted, or in the operation window, matching points should fine-tuned by a crosshair cursor until the total RMS value is less than 1 pixel and the matching points are evenly distributed. Finally, the output path and file name are selected to output the registered image.

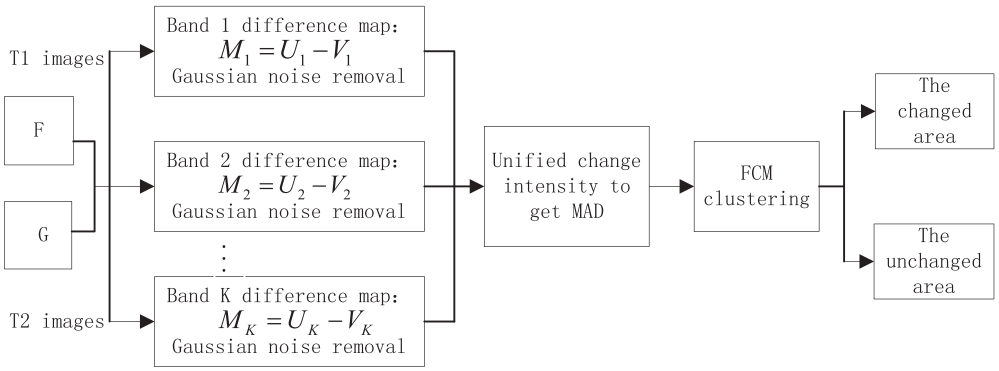

Figure 1. Flowchart of the designed framework.

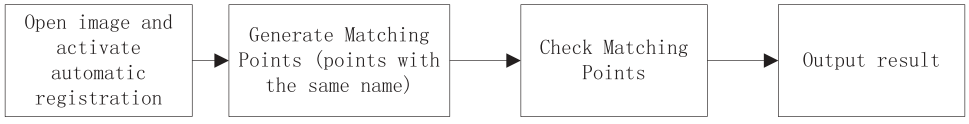

Figure 2. Flowchart for registration by ENVI.

Single band iterative weighting algorithm

The idea of single-band iterative weighting is as follows: First, the single-band image is extracted from the multi-spectral image. Second, the image is individually weighted by iteration for each band to obtain a projection vector that maximizes the correlation coefficient of each single-band image. Third, the optimal MAD variable of the band is obtained. In this way, the obtained MAD variables have the most abundant change information in each band. Finally, the final change-intensity map is generated after the fusion of the change intensities. The specific implementation method is as follows:

(1) Extract a single-band image from multi-spectral images $\boldsymbol{F}_1, \boldsymbol{F}_2, \ldots \boldsymbol{F}_K$ and a single-band image from multi-spectral images $\boldsymbol{G}_1, \boldsymbol{G}_2, \ldots \boldsymbol{G}_K$.
(2) Find a projection vector that maximizes the correlation coefficient of each single-band image. Let the vector of the *Pth* band image be optimally projected as $\boldsymbol{U}_P$ and $\boldsymbol{V}_P$, as shown in Equations (1) and (2):

$$\boldsymbol{U}_P = a_P^T \boldsymbol{F}_P \tag{1}$$

$$\boldsymbol{V}_P = b_P^T \boldsymbol{G}_P \qquad P = 1 \ldots K \tag{2}$$

where P is the corresponding number of bands, and $a_P$and b_P represent the projection vectors of the P-band images F and G, respectively. The projection vectors a_P and b_P can be found through Equations (3) and (4):

$$\sum\nolimits_{\boldsymbol{F}_P\boldsymbol{G}_P} \sum\nolimits_{\boldsymbol{G}_P\boldsymbol{G}_P}^{-1} \sum\nolimits_{\boldsymbol{G}_P\boldsymbol{F}_P} a_P = \rho^2 \sum\nolimits_{\boldsymbol{F}_P\boldsymbol{F}_P} a_P \tag{3}$$

$$\sum\nolimits_{\boldsymbol{G}_P\boldsymbol{F}_P} \sum\nolimits_{\mathrm{F}_P\boldsymbol{G}_P}^{-1} \sum\nolimits_{\boldsymbol{G}_P\boldsymbol{G}_P} b_P = \rho^2 \sum\nolimits_{\boldsymbol{G}_P\boldsymbol{G}_P} b_P \tag{4}$$

where $\rho = \mathrm{Corr}\left(a_P^T \boldsymbol{F}_P, b_P^T \boldsymbol{G}_P\right)$ represents the correlation of two eigenvectors. $\sum_{\boldsymbol{F}_P\boldsymbol{F}_P}$ is the covariance matrix of the P-band image between the multi-spectral image $\boldsymbol{F}$. $\sum_{\boldsymbol{G}_P\boldsymbol{G}_P}$ is the covariance matrix of the P-band image of the multi-spectral image $\sum_{\boldsymbol{F}_P\boldsymbol{G}_P}$ and $\sum_{\boldsymbol{G}_P\boldsymbol{F}_P}$ is the cross-covariance matrix between two P-band images. The MAD variable M_P generated by a single band is expressed as shown in Equation (5):

$$\boldsymbol{M}_P = \boldsymbol{U}_P - \boldsymbol{V}_P = a_P^T \boldsymbol{F}_P - b_P^T \boldsymbol{G}_P \tag{5}$$

The MAD feature satisfies the properties of the Gaussian distribution. Hence, the chi-square distance of the difference image can be calculated, which satisfies a chi-square distribution with n degrees of freedom, as shown in Equation (6):

$$T_{ij} = \left(\frac{M_{ij}^P}{\sigma^P}\right)^2 \in x^2(n) \tag{6}$$

where σ^P is the variance of the P-th band, and the weight is calculated by the probability density quantile of the chi-square distribution:

$$\omega_{ij} = P\left(T_{ij} > t\right) = P\left(x^2(n) > T_{ij}\right) \tag{7}$$

In the next iteration of the corresponding P-band image, the calculation of the mean and variance considers the effect of the weight. When the set number of iterations is reached, or the difference between the maximum eigenvalue before and after the iteration is less than 10^{-6}, the iteration will be stopped.That is, the image of each band uses the respective correlation coefficients to find the projection vector and weight in the iterative calculation process.

3. Calculate the MAD variable intensity matrix. After iterative convergence, the optimal MAD variable of the P-band can be obtained. The best difference image M_P of each band can be obtained through this algorithm. After Gaussian filtering and denoising, the obtained difference matrix is adjusted into the column vector by band. In matrix $\boldsymbol{M}$ (Equation (8)):

$$\boldsymbol{M} = (\boldsymbol{M}_1, \boldsymbol{M}_2, \ \ldots \ \boldsymbol{M}_K) \tag{8}$$

$$\mathrm{MAD} = \sqrt{\sum\nolimits_{K=1}^{P} (\boldsymbol{M} \cdot \boldsymbol{M})} \tag{9}$$

The Euclidean distance (Equation (9)) is used to convert the difference matrix into the MAD change-intensity matrix, and the intensity of the change in the pixels in each band is unified.

Difference map

For images of different time phases in the same area, how to accurately acquire the difference image of two-phase remote sensing images is very important in the multi-spectral remote sensing image change detection algorithm. The quality of different images will directly affect the accuracy of the classification results. The IR-MAD algorithm has been considered the most advanced change detection algorithm for multiphase images due to its excellent change detection accuracy and varying stability. However, the IR-MAD algorithm is a change detection algorithm based on the maximum variance of the projection difference, and the algorithm still has some shortcomings. In the process of calculation, bands with a weak correlation are positioned in front to assign small weights, while bands with a strong correlation were positioned at the back to assign large weights. If the weight is taken as the step length for adjusting the correlation coefficient, a band with a strong correlation will converge more rapidly due to the large

correlation coefficient. Moreover, a band with a small step length and weak correlation will stop the iteration due to the convergence of the band with the strong correlation. Therefore, the band with a weak correlation cannot converge to a large correlation coefficient, and the change information contained in the band cannot be fully utilized. Hence, a band with a weak correlation contributes less when the difference graph is obtained. The single-band iterative weighting algorithm can avoid this disadvantage and enhance the correlation coefficients of weak correlation bands, making full use of the change information of each band to improve the change detection accuracy. Data II is taken as an example to compare the feature-difference maps of each band obtained by the IR-MAD algorithm and the algorithm in this paper under the same number of iterations. The experimental results are as follows:

Figure 3 is the characteristic difference image of the six bands obtained after 10 iterations of the IR-MAD algorithm in Data II. The output bands are arranged from smallest to largest according to the characteristic correlation of the band. That is, Figure 3(a) corresponds to the band with the minimum correlation coefficient, and Figure 3(f) corresponds to the band with the maximum correlation coefficient. Panels (a), (b), (c), (d), (e) and (f) in Figure 3 correspond to the original bands for Band 3, Band 4, Band 5, Band 6, Band 2 and Band 1. In Figure 4(a), the RGB images were synthesized from the first three bands in Figure 3. Figure 4(b) is the RGB image synthesized in the last three bands in Figure 3. From Figure 3, it can be seen that the lower the MAD feature ranking was, the more abundant the change information became. That is, the larger the feature correlation ρ was, the more abundant the change information became. Figure 4 shows that the feature-difference of the band with a small correlation coefficient in the front contains more noise and background information, while the band with a large correlation coefficient in the back contains more change information and less noise. Therefore, there is a need to increase the correlation coefficient of each wave band through iterations.

Figure 5 is the feature-difference image of each band after 10 iterations using the single-band iterative weighting method. The serial number of the image is consistent with the band number. Figure 6(a) shows the RGB image synthesized by Band 3, Band 4 and Band 5. Figure 6(b) shows the RGB image synthesized by Band 6, Band 2 and Band 1 (consistent with the bands used in Figure 4). Table 1 is the first correlation value of each band after 10 iterations using the IR-MAD algorithm and the single-band iterative weighting method, respectively, in Data II. As shown in Figure 5, after single-band iterative weighting, the change information of each band is very clear. Compared with Figure 4, Figure 6(a) presents the clearer colour composite image, which was originally vague with change information. The single-band

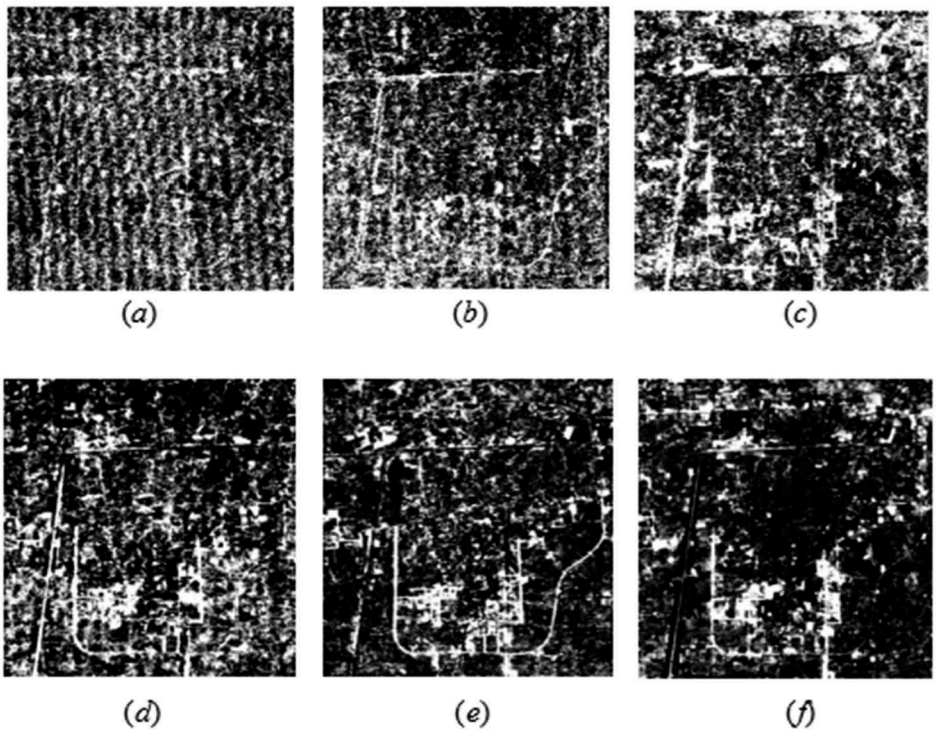

Figure 3. Output characteristic difference obtained using the IR-MAD algorithm (feature band 1–6).

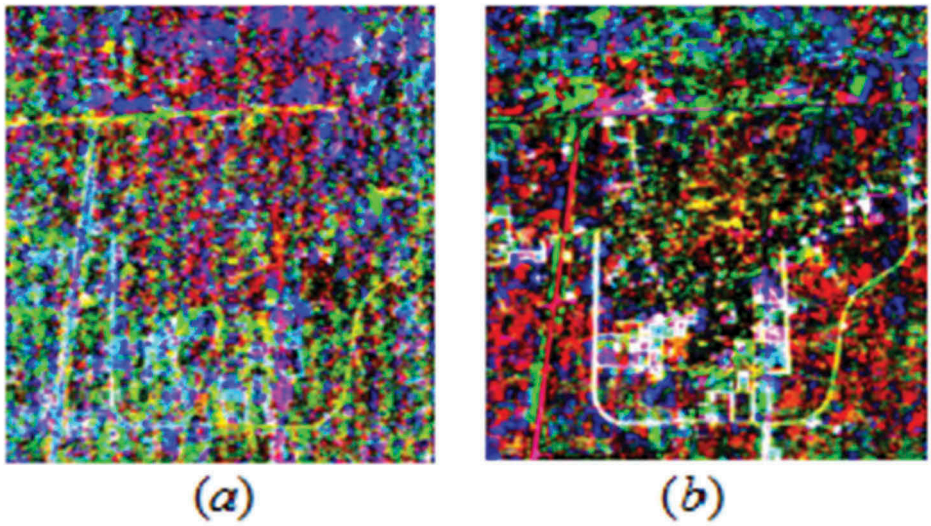

Figure 4. (a) Color synthesis map of the first three characteristic bands of the IR-MAD algorithm, and (b) Color synthesis of the last three characteristic bands.

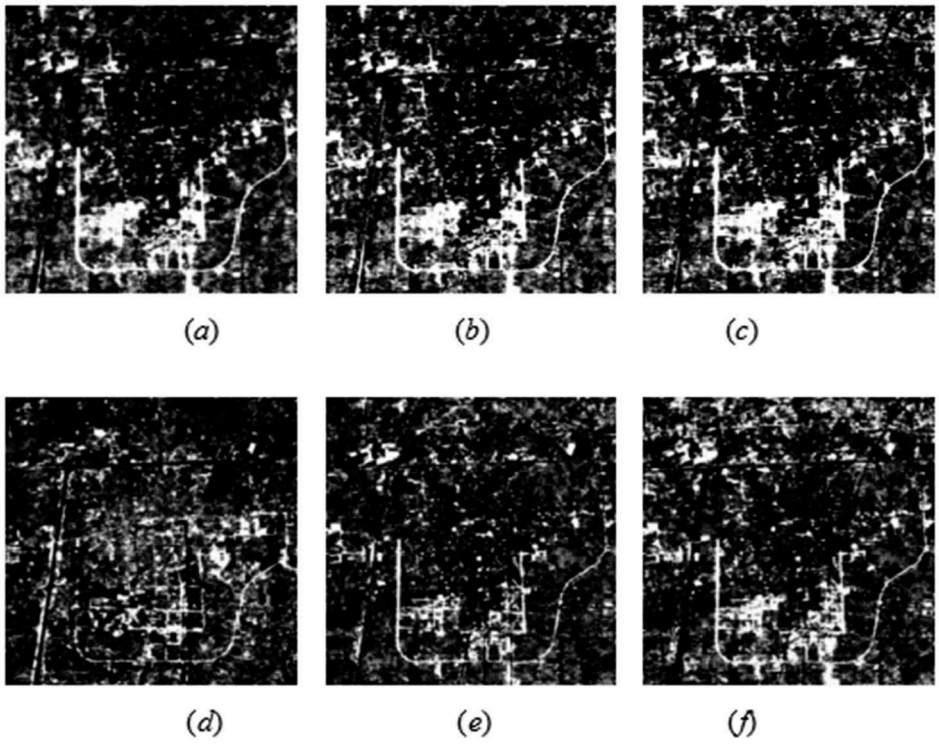

Figure 5. Output characteristic difference obtained by the single-band iterative weighting algorithm (feature band 1–6).

iterative weighted method significantly enhanced the correlation of Band 3, Band 4 and Band 5, which were originally weak in correlation. The data in Table 1 are also very good for proving this relationship. Therefore, the single-band iterative weighting method can effectively enhance the correlation coefficient of the bands with weak correlation. Hence, the change information of the band can also be fully utilized to improve the accuracy of change detection.

FCM clustering algorithm

To extract change information from different images, traditional algorithms include thresholding and clustering, which take into account the statistical characteristics of images and can complete the classification well. In this paper, the FCM clustering algorithm is used to cluster the acquired MAD difference image to obtain the final change detection map. This clustering algorithm aims at minimizing the objective function, which is defined as:

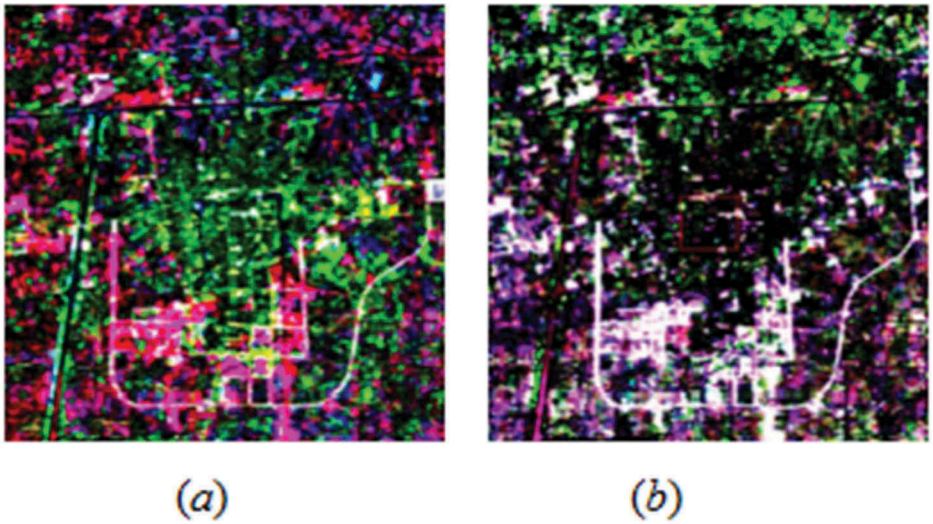

Figure 6. Color synthesis map of the single-band iterative weighting algorithm: (a) shows the RGB image synthesized by band 3, band 4 and band 5; (b) shows the RGB image synthesized by band 6, band 2 and band 1.

Table 1. The correlation coefficient values of each band after processing.

	Band3	Band4	Band5	Band6	Band2	Band1
10 iterations by IR-MAD (ρ)	0.475	0.6811	0.78	0.8886	0.9696	0.9872
10 iterations by single-band weighting (ρ)	0.9978	0.9988	0.9989	0.9981	0.9971	0.9967

$$J_m = \sum_i^c \sum_j^n (u_{ij})^m ||y_j - z_i||^2 = \sum_i^c \sum_j^n (u_{ij})^m d_{ij}^2 \tag{10}$$

where $Y = (y_1, y_2, \ldots, y_n)$is a set of n-dimensional data samples, $Z = (z_1, z_2, \ldots, z_c)$ is the clustering centre of the fuzzy group, $U = [u_{ij}]_{c\times n}$is the membership matrix of Y and $u_{ij}\epsilon[0,1].d_{ij} = ||z_i - y_j||$ is the Euclidean distance between the ith clustering centre and the jth data point, and $m = [1, \infty)$is a weighted index, which represents the fuzzy index. Its size is proportional to the degree of blurring. Generally, its standard value is 1.5. The necessary conditions for reaching the minimum value of J_m can be obtained by the Lagrange multiplier:

$$z_i = \frac{\sum_{j=1}^n u_{ij}^m y_j}{\sum_{j=1}^n u_{ij}^m}, \qquad 1 \le i \le c \tag{11}$$

$$u_{ij} = \frac{1}{\sum_{k=1}^c \left(\frac{d_{ij}}{d_{kj}}\right)^{\frac{2}{(m-1)}}}, \qquad 1 \le i \le c, 1 \le j \le n \tag{12}$$

where,

$$\sum_{i=1}^c u_{ij} = 1, \forall_j = 1, \ldots, n \tag{13}$$

It can be seen from the two necessary conditions above that the FCM clustering algorithm is an iterative process. Equations (11) and (12) are iteratively repeated to satisfy the condition and obtain the final clustering result.

Experimental results and comparisons

To verify the superiority of the proposed algorithm, this paper uses three sets of Landsat multi-spectral remote sensing data for experimental verification. The detection results obtained by different algorithms were compared from subjective and objective indicators. The objective indicators include the number of false negatives (FN), the number of false positives (FP), the overall error (OE), the percentage correct classification (PCC) (Gao, Liu, Dong, Zhong, & Jian, 2017), and the Kappa coefficient (KC) (Rosin & Ioannidis, 2003). FN indicates the number of pixels that were originally a changed class and are detected as an unchanged class; FP indicates the number of pixels that were originally an unchanged class and are detected as a changed class; OE represents the sum of the number of false alarms and missed detections; PCC indicates the proportion of correctly classified samples to the total number of samples. The closer the PCC is to 1, the better the change detection performance. KC is a more accurate measurement of the classification accuracy. The value of the parameter is primarily used to measure the similarity between the change result graph and the reference image. The ideal value is 1, which means that the test result is completely consistent with the reference image (Gong, Zhou, & Ma, 2012).

Experimental data I

Data I is a manual simulation data set.The remote sensing image of phase 1 was taken by Landsat 5 TM in 2011, and it is a multi-spectral image of the Changji region in Xinjiang. The remote sensing image of phase 2 was simulated by manually adding changing regions to the multi-spectral remote sensing image of phase 1. The specific method of addition is as follows: A region A of a certain size is captured from the Band 1 image, and A is replaced by region B, which contains different ground object information (i.e., A is the same size as B and contains different ground object information) to simulate the changing region. This method is used to obtain the Band 1 images of phase two and process the remaining bands equally (the positions of the intercepting and replacement regions are completely consistent with Band 1). In this way, single-band processing can guarantee the consistency of the ground features of each band. Then, the simulated phase two multi-spectral images can be obtained. The obtained multi-temporal Landsat multi-spectral image has many advantages. (1) They are not affected by clouds, weather, etc. Hence, registration is not required. (2) Since the pixel values are completely consistent, except for the change area, the detection is almost completely free from noise. (3) As the change area is manually added, it is convenient to make the change reference graph for the objective analysis of the test results. Therefore, the simulation of multi-spectral image change with this method can be used to identify the advantages and disadvantages of the algorithm. Figure 7(a) shows the pseudo-colour composite image of size 250 × 250 pixels of the multi-spectral data in the Changji area of Xinjiang in 2011. Figure 7(b) shows the pseudo-colour composite image after manually adding the change area to Figure 7(a). The change reference map is presented in Figure 7(c).

The data set was used for change detection experiments, and the detection results of the proposed algorithm are compared with the detection results of MAD, IR-MAD, and the mask elimination strong-change method.The experimental results were as follows. Figure 8 shows the MAD algorithm, IR-MAD algorithm, mask elimination strong-change method, and the single-band iterative weighting method proposed in the present study. From the results graph, we can see that there are more broken plaques in the MAD algorithm detection results, and some details of the changes are not well detected. The IR-MAD algorithm and the algorithm with masking have slightly improved the effect, but there are still more broken plaques. The detection result of the proposed method is closest to the reference picture.

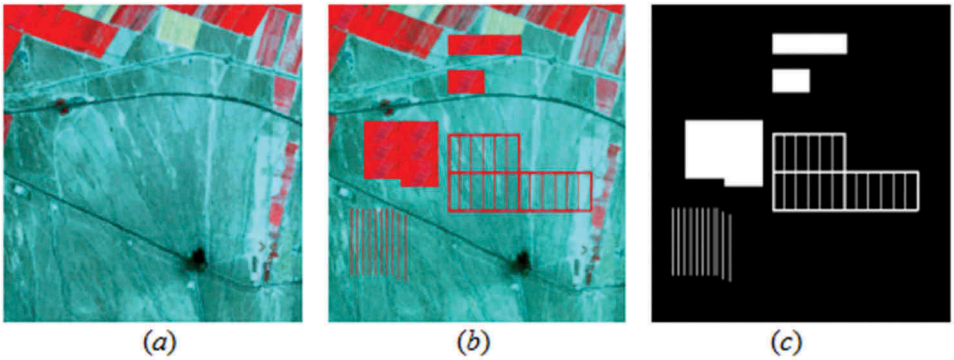

Figure 7. (a) Pseudo-color composite image of the multispectral data. (b) Pseudo-color composite image of (a) the multispectral data change simulation. (c) The reference change image.

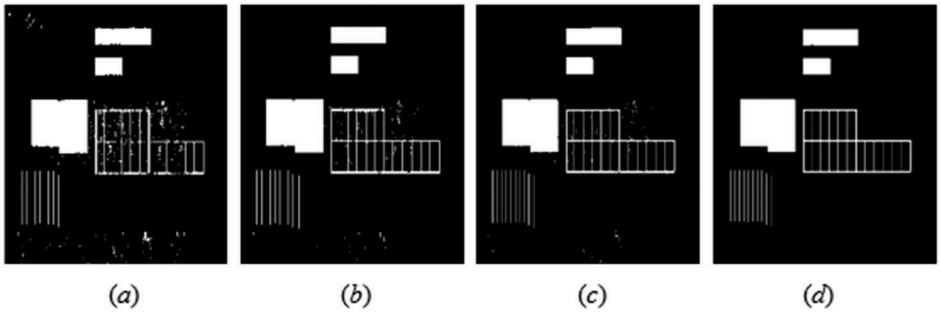

Figure 8. Change detection image obtained for the Changji simulated data set: (a) MAD; (b) IR-MAD; (c) masking to eliminate strong changes; (d) single-band iterative weighting.

Table 2. The multi-spectral image change detection results evaluated by different algorithms.

Method Used	FN	FP	OE	PCC(%)	KC
MAD	162	553	715	0.9886	0.9389
IR-MAD	23	185	208	0.9967	0.982
With Mask	17	168	185	0.997	0.9839
Proposed Method	13	1	14	0.9998	0.9989

Table 3. The multi-spectral image change detection results evaluated by different algorithms.

Method Used	FN	FP	OE	PCC(%)	KC
MAD	599	28445	29044	0.8185	0.1607
IR-MAD	560	18455	19015	0.8812	0.2448
With Mask	906	9018	9924	0.938	0.3764
Proposed Method	391	7581	7972	0.9502	0.47

Table 2 presents the objective evaluation values of the obtained detection results (the overall detection accuracy of each algorithm is relatively high due to the no noise and registration errors). In Table 2, it can be seen that the total numbers of missed detections FN and false alarms FP in the detection result of the single-band iterative weighting algorithm was the lowest and are much less than those of the other three algorithms. The PCC and KC values were also the highest. From Data I and the present test results, the algorithm proposed in the present study exhibited a higher detection precision, both in the detection of large-change regions and more detailed regions.

Experimental data II

Date II was acquired by Landsat 7 on 17 March 2000, and 6 February 2003. The region of interest was located in Taizhou City, Jiangsu Province, China. The image size was 400 × 400 pixels, including six bands. The two remote sensing images shown in Figure 9(a and b) are the pseudo-colour synthesis of Band 4 (red band), Band 3 (green band), and Band 2 (blue band). The change reference map is presented in Figure 9(c).

As shown in Figure 10, it can be seen from the experimental results that with (a), the numbers of missed detections FN and false alarms FP of the algorithm are relatively large. Hence, the value of OE is relatively large, and PCC and KC are both relatively low. The error in the test results is relatively large. When (b) was compared with (a), the algorithm exhibited a great improvement in leak detection and false alarms, and the accuracy of the PCC and KC values improved, but the detection accuracy was still not high overall. Through the experimental results in (c), it can be seen that the changes were under the circumstances of fewer pixels, and the use of a mask to eliminate the variation in the improved algorithm allowed for more recognition and did not change the pixels. Furthermore, the PCC and KC values improved, but the total number of fault detection OE was on the large

Figure 9. Taizhou ETM+ data pseudo-color composite image. (a) 2000 and (b) 2003; (c) Test sample of the Taizhou image. The background samples were black, the unchanged samples were gray, and the change samples were white.

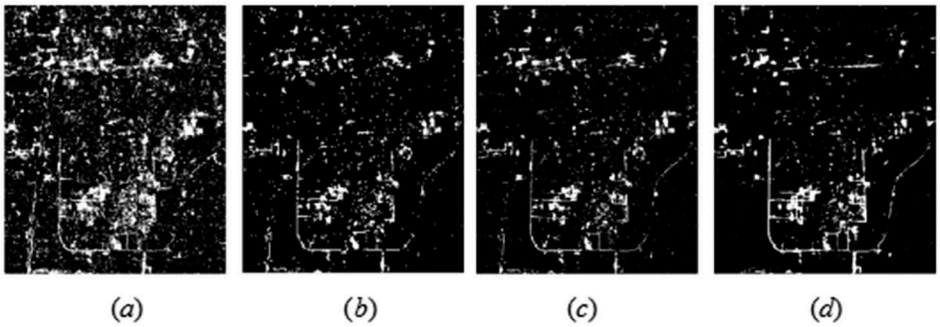

Figure 10. The change detection image obtained for the Taizhou data set: (a) MAD; (b) IR-MAD; (c) masking to eliminate strong changes; (d) single-band iterative weighting.

side. Hence, considering the accuracy, it could not achieve an obvious improvement. The experimental results of Table 3 show that the single-band iterative weighting algorithm (d) was considered. The PCC was 0.07 higher than that of the original algorithm (b). The KC value was 0.23 higher than that of the original algorithm (b). From the detection accuracy, it can be seen that the change detection result was significantly higher than that of (b), which shows a better, improved algorithm.

Experimental data III

Data III was acquired in Changji, Xinjiang. The phase one image is a multi-spectral image taken by Landsat 5 TM (Sulla-Menashe, Friedl, & Woodcock, 2016) in 2011. There are seven bands in total, and six visible and near-infrared bands, except for the thermal infrared band (TM6), were selected. During phase two of the images taken in 2014 by Landsat 8 OLI (Wei & Yan-Tao, 2015), there were a total of 11 bands, which were chosen corresponding to the cross section (Band 2), green band (Band 3), red band (Band 4), near-infrared band (Band 5), shortwave infrared band 1 (Band 6), and shortwave infrared band 2 (Band 7). Then, the original image was geometrically registered, and an extraction area of 500 × 500 pixels was used as the research object. Figure 11(*a*) presents the standard pseudo-colour image synthesized with Band 4 (red band), Band 3 (green band), and Band 2 (blue band) in the multi-spectral image taken by Landsat 5 TM in 2011. In Figure 11(*b*), a standard pseudo-colour image synthesized with Band 5 (near-infrared band), Band 4 (red band), and Band 3 (green band) in a multi-spectral image taken by Landsat 8 OLI in 2014 is shown. To facilitate the comparison of the test results, a typical area was selected for comparison, as shown in Figure 11(*c*), in which the red mark represents the change area, while the blue mark represents the unchanged area.

As shown in Figure 12, it can be seen from the detection results that algorithm (*a*) classifies many unchanging pixels as changing pixels (the reference region of blue markings), and the detection results are greatly affected by noise. Algorithm (*b*) iterates 20 times, and the convergence detection effect is better than that of (*a*), but the changes in the details are not detected. At the same time, there are some false alarm points in the detection results. Algorithm (*c*) converges after five iterations, which is much less than those of (*b*), and the convergence speed is faster. It can be seen from the experimental results that the mask used in the case of a large number of changed pixels can significantly accelerate the convergence speed and better converge to the unchanging background. However, some minor changes were missed. Algorithm (*d*) was weighted by 20 iterations in

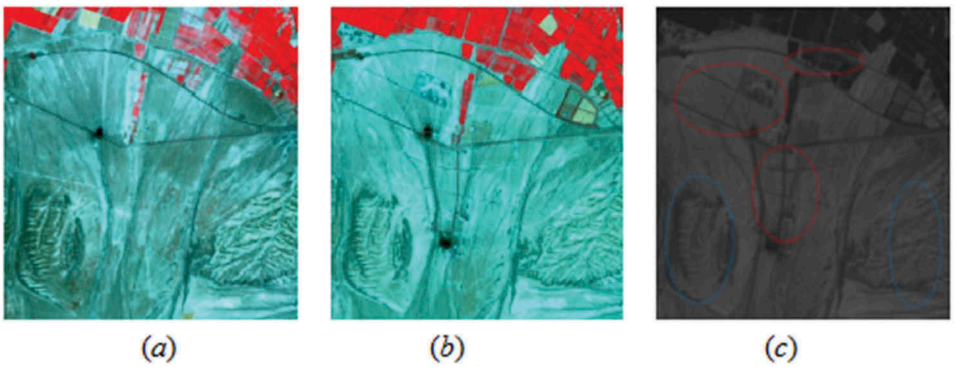

Figure 11. Pseudo-color composite image of multi-spectral data in Changji, Xinjiang. (a) 2011 and (b) 2014; (c) labeled reference area.

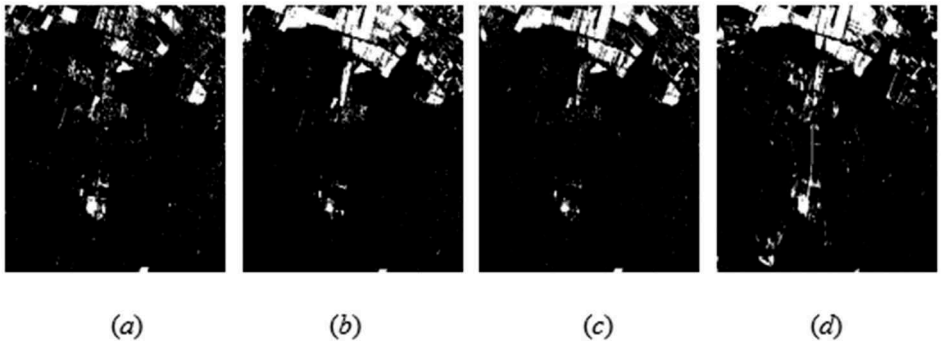

Figure 12. Change detection image obtained for the Changji data set: (a) MAD; (b) IR-MAD; (c) masking to eliminate strong changes; (d) single-band iterative weighting.

a single band, allowing each band to make a great contribution to the acquisition of the change-intensity graph. From the experimental results, it can be seen that even small changes can be detected, and better detection results can be obtained, which indicates a good, improved algorithm.

Discussion

To discuss the influence of Gauss denoising on the detection accuracy before and after the improvement of the IR-MAD algorithm, we take Data II as an example. Experiments were also carried out under the condition of 10 iterations and the FCM clustering algorithm. To improve the accuracy of the data, the average PCC and KC values obtained by 20 change detections were taken. The histogram obtained from the experimental results is shown in Figure 13.

Comparing the results of the IR-MAD and GS IR-MAD algorithms in the comparison chart (Figure 8) and the detection results of SBIW and GS SBIW, it can be seen that under the same detection algorithm, Gaussian denoising can perform simple denoising on the image to a certain extent, and it can improve the detection accuracy. Comparing the detection results of the IR-MAD and SBIW algorithms and the detection results of the GS IR-MAD and GS SBIW algorithms, we can see that the single-band iterative weighting algorithm has obvious advantages in acquiring the difference graph, which proves that the proposed algorithm has a higher detection accuracy than the other algorithms.

Table 4. Results of detecting the average change of multispectral remote sensing images.

Method Used	FN	FP	OE	PCC(%)	KC
MAD	120	275	395	0.984	0.9372
IR-MAD	113	195	308	0.9882	0.9519
With Mask	158	70	228	0.9912	0.962
Proposed Method	72	8	80	0.9968	0.9872

To verify the universality of the algorithm, 100 sets of Landsat 5 TM datasets were created by manually adding varying regions. Change detection was conducted by the proposed method, and a comparison was made between the original MAD algorithm, the IR-MAD algorithm and the proposed IR-MAD algorithm, which used a mask to eliminate strong changes. The average PCC and KC values of the 100 datasets were obtained, and the results are shown in Table 4.

Table 4 shows that the average total error detection (OE) of the proposed algorithm was the lowest. It can be seen from the mean of the PCC and KC values that the single-band iterative weighting method is superior to other algorithms in terms of the detection accuracy. The KC value of the proposed method is 5% higher than that of the MAD algorithm, 3.53% higher than that of the IR-MAD algorithm, and 2.52% higher than that of the masking algorithm. Through the experiment with 100 sets of data, the superiority of the single-band iterative weighting algorithm was fully

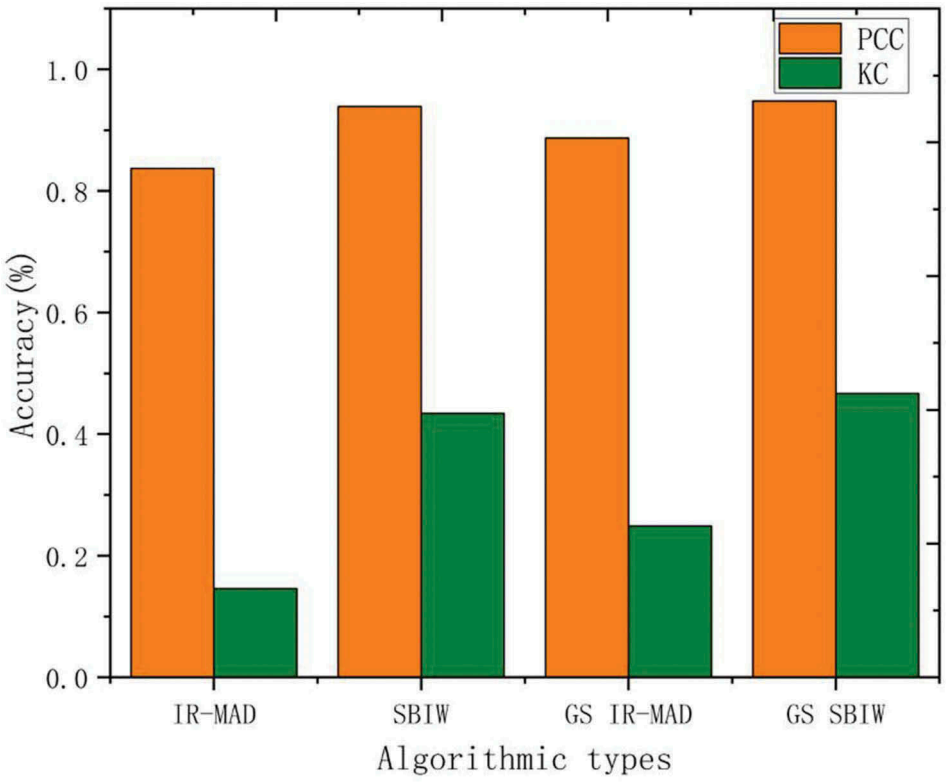

Figure 13. Accuracy comparison histogram.

verified. Hence, the single-band iterative weighting method exhibits good universality.

Conclusion

A new multi-spectral change detection algorithm is proposed in this article to improve the contribution of weakly correlated bands in multi-spectral image change detection. The image weights of each band were set to different weights to improve the correlation between each pair of bands of multi-spectral images. This method was used to obtain the characteristic difference diagrams of each band that contained more variation information. After removing Gaussian noise in each feature-difference graph, the difference graphs of each band were fused into a change-intensity graph using the Euclidean distance formula. Finally, unsupervised FCM binary clustering was used to divide the difference map into two categories. Experiments on real multi-spectral image datasets show that our approach can improve change detection results. Compared with the detection results obtained by the reference methods, the detection results obtained by the proposed algorithm are greatly improved in terms of the visual effect and objective quantitative indices.

Disclosure statement

No potential conflict of interest was reported by the authors.

Funding

This research was supported by [the National Science Foundation of China] under grant number [No. 61665012]; and [the International Cooperative Research and Personnel Training Projects of the Ministry of Education of the People's Republic of China] under grant number [No. 2014-2029 and 2016-2196].

References

Bai, M., Liu, H.P., Zhu, S.D., & Feng, H.H. (2012). Relative radiometric correction for remote sensing images based on multivariate alteration detection. *Science of Surveying & Mapping*. Beijing, China.

Canty, M.J., & Nielsen, A.A. (2008). Automatic radiometric normalization of multitemporal satellite imagery with the iteratively re-weighted MAD transformation. *Remote Sensing of Environment*, *112*(3), 1025–1036. doi:10.1016/j.rse.2007.07.013

Chen, Q., & Chen, Y. (2016). Multi-feature object-based change detection using self-adaptive weight change vector analysis. *Remote Sensing*, *8*(7), 549. doi:10.3390/rs8070549

Gao, F., Liu, X., Dong, J., Zhong, G., & Jian, M. (2017). Change detection in SAR images based on deep semi-NMF and SVD networks. *Remote Sensing*, *9*(5), 435. doi:10.3390/rs9050435

Gong, M., Niu, X., Zhang, P., & Li, Z. (2017). Generative adversarial networks for change detection in multispectral imagery. *IEEE Geoscience & Remote Sensing Letters*, *14*(12), 2310–2314. doi:10.1109/LGRS.2017.2762694

Gong, M., Yang, Y., Zhan, T., Niu, X., & Li, S. (2019). A generative discriminatory classified network for change detection in multispectral imagery. *IEEE Journal of Selected Topics in Applied Earth Observations and Remote Sensing*, *PP*(99), 1–13.

Gong, M., Zhao, J., Liu, J., Miao, Q., & Jiao, L. (2017). Change detection in synthetic aperture radar images based on deep neural networks. *IEEE Transactions on Neural Networks & Learning Systems*, *27*(1), 125–138. doi:10.1109/TNNLS.2015.2435783

Gong, M., Zhou, Z., & Ma, J. (2012). Change detection in synthetic aperture radar images based on image fusion and fuzzy clustering. *Image Processing IEEE Transactions On*, *21*(4), 2141–2151. doi:10.1109/TIP.2011.2170702

Hichri, H., Bazi, Y., Alajlan, N., & Malek, S. (2013). Interactive segmentation for change detection in multispectral remote-sensing images. *IEEE Geoscience & Remote Sensing Letters*, *10*(2), 298–302. doi:10.1109/LGRS.2012.2204953

Hui, Z. (2008). A SAR image change detection algorithm based on principal component analysis. *Journal of Electronics & Information Technology*, *30*(7), 1727–1730.

Jian, Z., Fang, L., & Ghamisi, P. (2018). Deformable convolutional neural networks for hyperspectral image classification. *IEEE Geoscience & Remote Sensing Letters*, 15(8), 1–5. doi:10.1109/LGRS.2018.2830403.

Lei, C., & Run-Geng, M.A. (2007). Detection of remote sensing image alteration based on canonical correlation analysis. *Geological Bulletin of China*, *292*(1), 237–243.

Liang, L.I., Wang, L., Sun, X., & Ying, G. (2017). Remote sensing change detection method based on object-oriented change vector analysis. *Remote Sensing Information*, *32*(06), 71–77.

Maggiori, E., Tarabalka, Y., Charpiat, G., & Alliez, P. (2016). Convolutional neural networks for large-scale remote sensing image classification. *IEEE Transactions on Geoscience & Remote Sensing*, *55*(2), 645–657. doi:10.1109/TGRS.2016.2612821

Marpu, P.R., Gamba, P., & Canty, M.J. (2011). Improving change detection results of IR-MAD by eliminating strong changes. *IEEE Geoscience & Remote Sensing Letters*, *8*(4), 799–803. doi:10.1109/LGRS.2011.2109697

Mishra, N.S., Ghosh, S., & Ghosh, A. (2012). Fuzzy clustering algorithms incorporating local information for change detection in remotely sensed images. *Applied Soft Computing Journal*, *12*(8), 2683–2692. doi:10.1016/j.asoc.2012.03.060

Mou, L., Bruzzone, L., & Xiao, X.Z. (2018). Learning spectral-spatial-temporal features via a recurrent convolutional neural network for change detection in multispectral imagery. *IEEE Transactions on Geoscience and Remote Sensing*, *PP*(99), 1–12.

Nielsen, A.A., & Canty, M.J. (2009). Kernel principal component and maximum autocorrelation factor analyses for change detection. *Image and Signal Processing for Remote Sensing XV*. doi: 10.1117/12.829645

Niemeyer, I., Marpu, P.R., & Nussbaum, S. (2008). *Change detection using object features* (pp. 185–201). Barcelona, Spain: Springer Berlin Heidelberg.

Qiao, J.F., Pan, G.Y., & Han, H.G. (2015). Design and application of continuous deep belief network. *Acta Automatica Sinica 41*(12), 2138-2146.

Rosin, P.L., & Ioannidis, E. (2003). Evaluation of global image thresholding for change detection. *Pattern*

Recognition Letters, *24*(14), 2345–2356. doi:10.1016/S0167-8655(03)00060-6

Roux, N.L., & Bengio, Y. (2008). Representational power of restricted {B}oltzmann machines and deep belief networks. *Neural Computation*, *20*(6), 1631–1649. doi:10.1162/neco.2008.04-07-510

Shi, A., Gao, G., & Shen, S. (2016). Change detection of bitemporal multispectral images based on FCM and D-S theory. *Eurasip Journal on Advances in Signal Processing*, *2016*(1), 96. doi:10.1186/s13634-016-0397-0

Song, W., Li, S., Fang, L., & Lu, T. (2018). Hyperspectral image classification with deep feature fusion network. *IEEE Transactions on Geoscience & Remote Sensing*, *56*(6), 3173–3184. doi:10.1109/TGRS.2018.2794326

Sulla-Menashe, D., Friedl, M.A., & Woodcock, C.E. (2016). Sources of bias and variability in long-term Landsat time series over Canadian boreal forests. *Remote Sensing of Environment*, *177*, 206–219. doi:10.1016/j.rse.2016.02.041

Wei, X.U., & Yan-Tao, X.I. (2015). Research on land use classification in hefei based on Landsat 8 images. *Hubei Agricultural Sciences*. Hubei, China.

Wu, C., & Du, B. (2015). *Research on multi-level information change detection of remote sensing images*. (PhD diss.). Wuhan University.

Xu, L., Zhang, S., He, Z., & Guo, Y. (2009). *The comparative study of three methods of remote sensing image change detection*. International Conference on Geoinformatics, Fairfax, VA, USA.

Xu, Q., Liu, Z., Li, F., Ren, H., & Yang, M. (2016). *The regularized iteratively reweighted object-based MAD method for change detection in bi-temporal, multispectral data*. Proceedings of the Spie, *156*. Beijing, China.

Yan-Hong, A.O., Pei, H., Wang, Y.L., & Yun-Peng, L.I. (2010). Monitoring on land cover dynamics of hunshandake sandland by remote sensing. *Journal of Desert Research*, *30*(1), 33–39.

Yonezawa, C. (2007). Maximum likelihood classification combined with spectral angle mapper algorithm for high resolution satellite imagery. *International Journal of Remote Sensing*, *28*(16), 3729–3737. doi:10.1080/01431160701373713

Zhang, J.X., & Yang, G.J. (2005). Automatic land use and land cover change detection with one temporary remote sensing image. *Journal of Remote Sensing*, *9*(3), 294-299.

Zhuang, H., Deng, K., & Fan, H. (2016). Filtering approach based on voter model and spatial-contextual information to the binary change map in SAR images. *Journal of the Indian Society of Remote Sensing*, *45*(5), 733–741. doi:10.1007/s12524-016-0639-5

Zhuang, H., Deng, K., Fan, H., & Ma, S. (2018). A novel approach based on structural information for change detection in SAR images. *International Journal of Remote Sensing*, *39*(8), 2341–2365. doi:10.1080/01431161.2017.1421794

Zhuang, H., Deng, K., Yu, Y., & Fan, H. (2017). An approach based on discrete wavelet transform to unsupervised change detection in multispectral images. *International Journal of Remote Sensing*, *38*(17), 4914–4930. doi:10.1080/01431161.2017.1331475